Iron complexes as electrocatalysts for the water oxidation reaction

Kottrup, K.G.

Appendix A

Supplementary information for Chapter 2

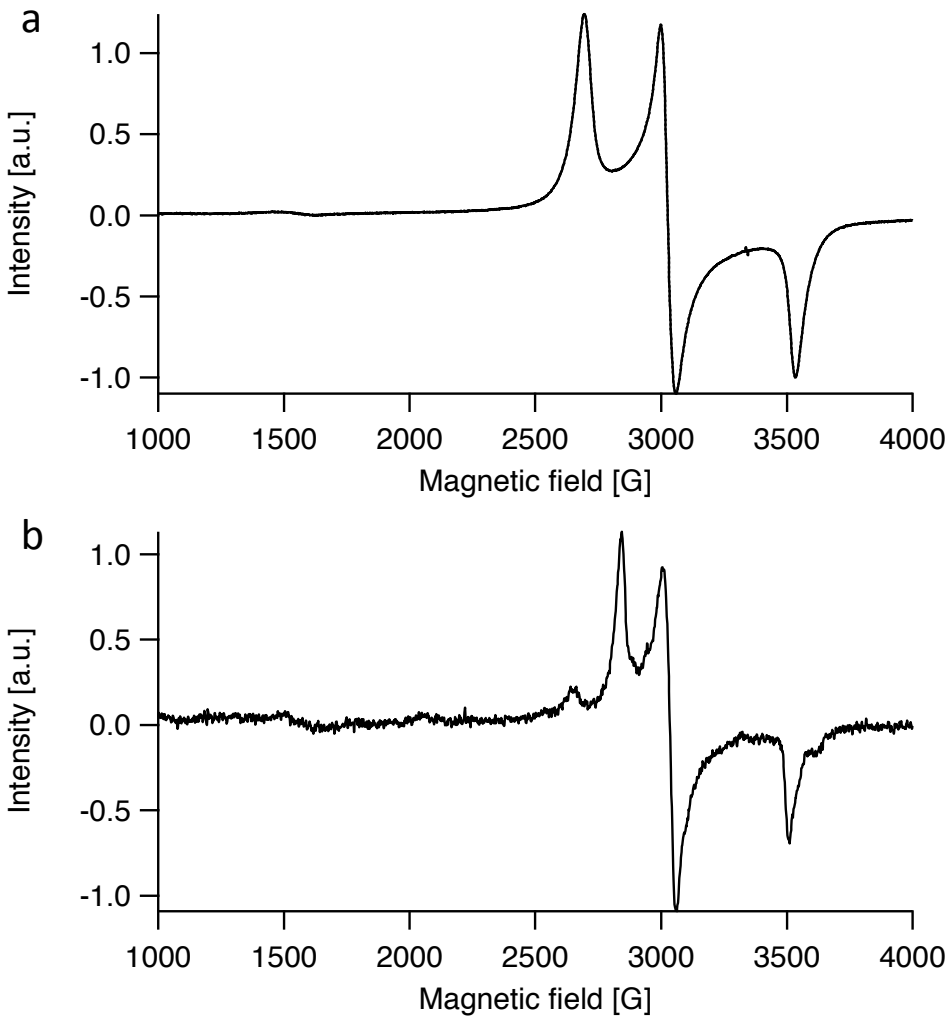

Figure A.1: X-band EPR spectra of the *in situ* oxidized complexes **2** and **3** in water/glycerol at 77 K. (a) Oxidized complex **2**; ν = 9.348 GHz; g-values: 2.48, 2.21, 1.89 (b) Oxidized complex **3**; ν = 9.354 GHz; g-values: 2.39, 2.24, 1.93

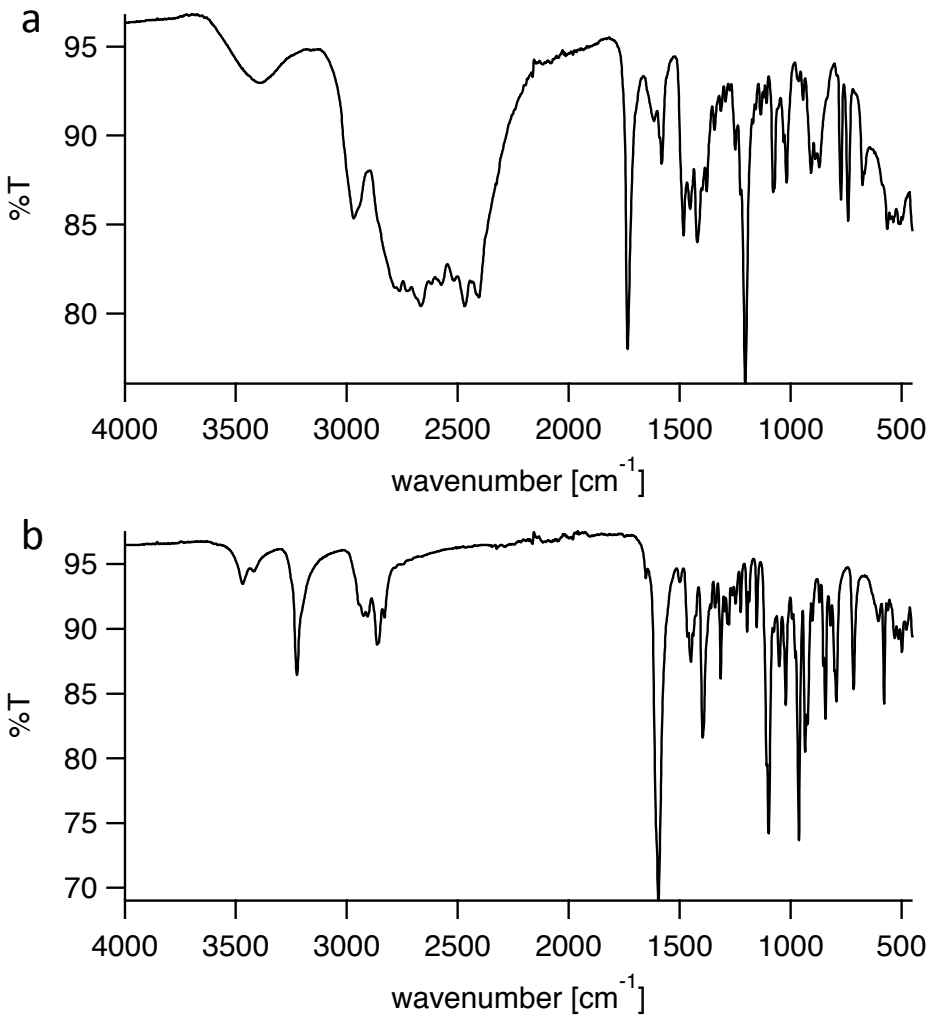

Figure A.2: IR spectrum of (a) cyclamacetate·4HCl (b) complex **2**; with C=O stretch frequencies of (a) 1734 cm^{-1} and (b) 1595 $cm^{-1.}$

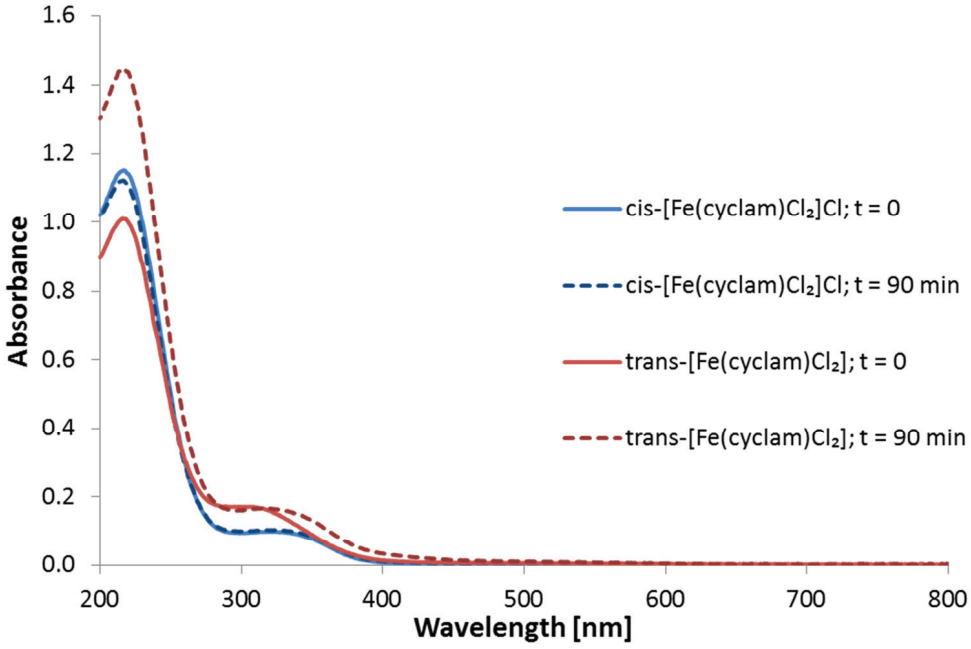

Figure A.3: UV-vis spectra of complexes **1** and **3** over time (t = 0 min → t = 90 min). Complex **1** is stable over the observed time span, whereas complex **3** changes noticeably within the first hour, likely due to oxidation from Fe^{II} to Fe^{III}. Both complexes give clearly different absorption spectra and show no signs of cis-trans-isomerization on the timescale of our experiments. Both complexes were used in identical concentrations of 0.11 mM.

Figure A.4: Solid material deposited onto the PG electrode surface during OLEMS measurement of complex **3** in 0.1 M phosphate buffer (pH 7.5)

Appendix B

Supplementary information for Chapter 3

B.1 Figures

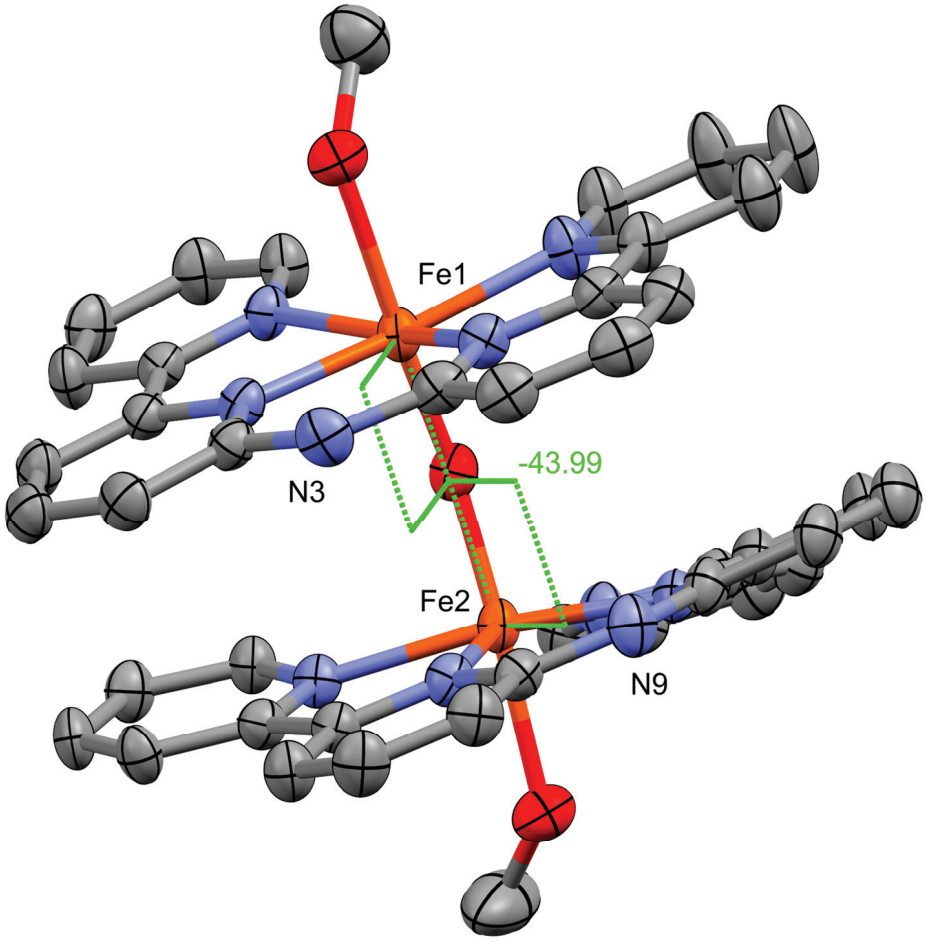

Figure B.1: Illustration of the offset between the two Hbbpya ligands in the crystal structure of [**1**]. Indicated is the torsion angle measured along N3-Fe1-Fe2-N9. Ellipsoids are shown with 50% probability. All hydrogen atoms and the four triflate counter-ions have been omitted for clarity.

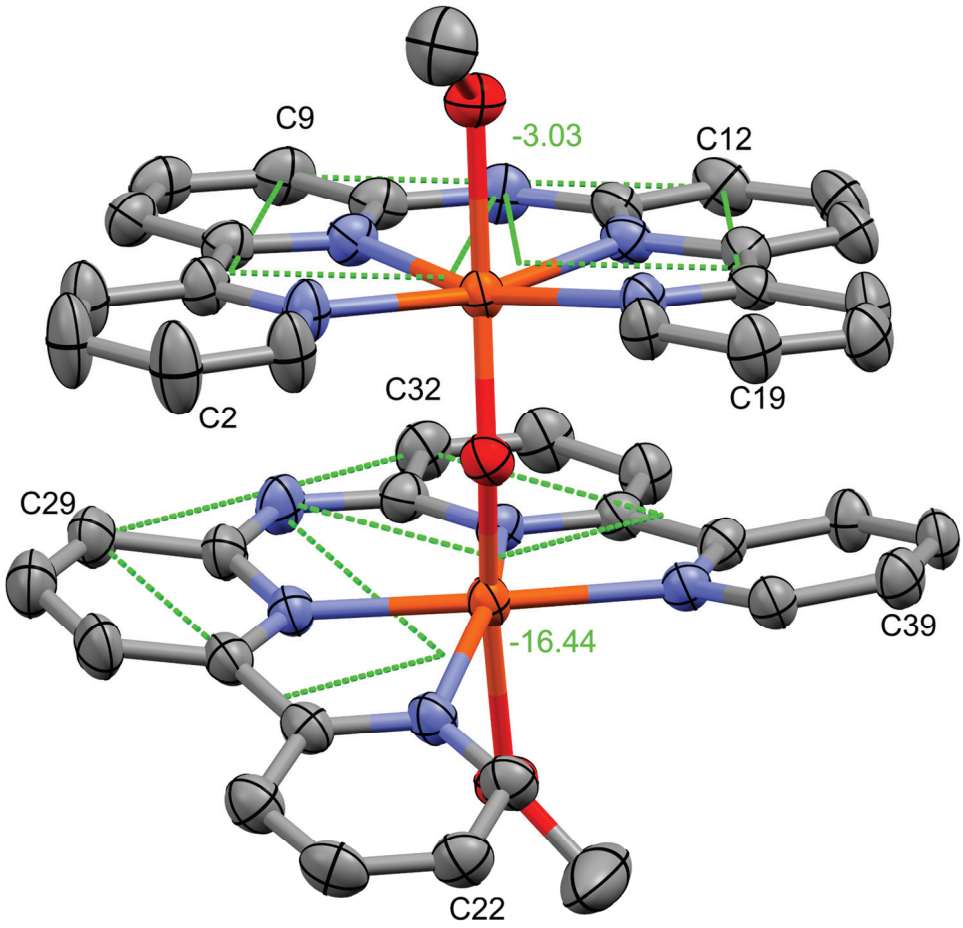

Figure B.2: Internal torsion angles of the two Hbbpya ligands in the crystal structure of [**1**]. The angles were calculated along C2-C9-C12-C19 and C22-C29-C32-C39 respectively which represent the respective 4 and 4' position carbon atoms of each bipyridine unit. Ellipsoids are shown with 50% probability. All hydrogen atoms and the four triflate counter-ions have been omitted for clarity.

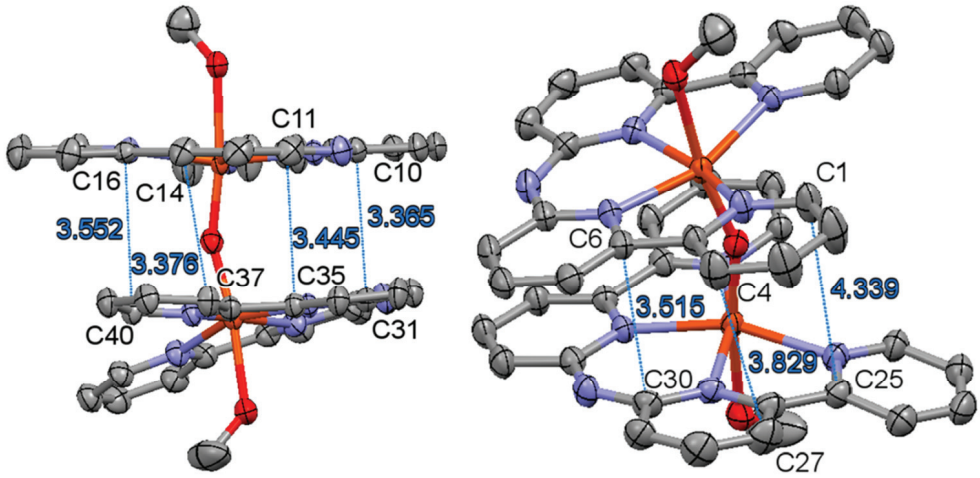

Figure B.3: Distances between the two Hbbpya ligands in the crystal structure of [**1**], measured between selected carbon atoms of the Hbbpya ligand. The pairs of carbon atoms in the measurements are: C1-C25, C4-C27, C6-C30, C10-C32, C11-C35, C14-C37 and C16-C40. Ellipsoids are shown with 50% probability. All hydrogen atoms and the four triflate counter-ions have been omitted for clarity.

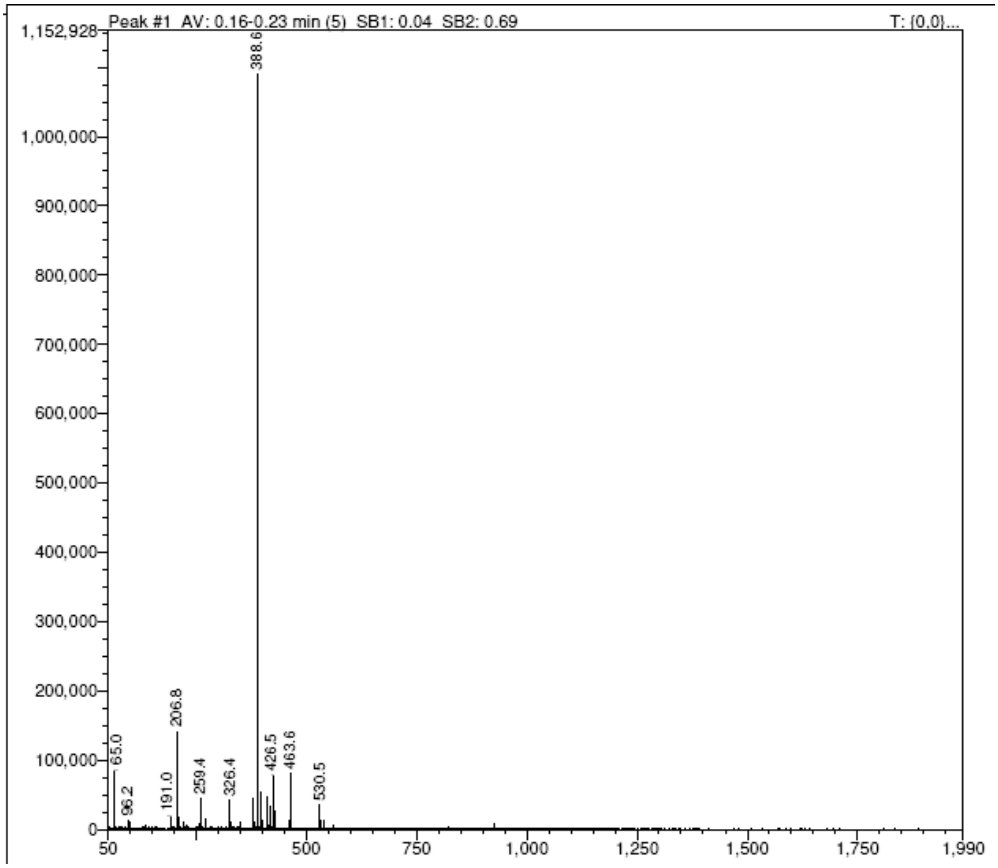

Figure B.4: ESI-MS spectrum of complex **1** in water. m/z = 388.6 corresponds to $[Fe^{III}(bbpya)–\mu\text{-}O–Fe^{III}(bbpya)]^{2+}$; calcd.: m/z = 388.1

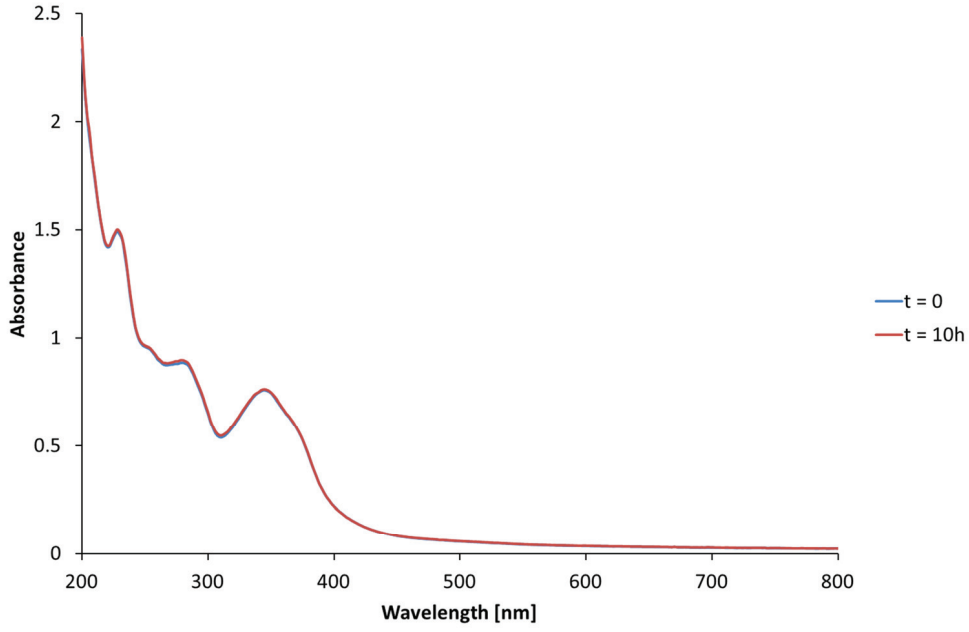

Figure B.5: UV-vis spectra of complex **1** in water at t = 0 (blue line) and t = 10 h (red line)

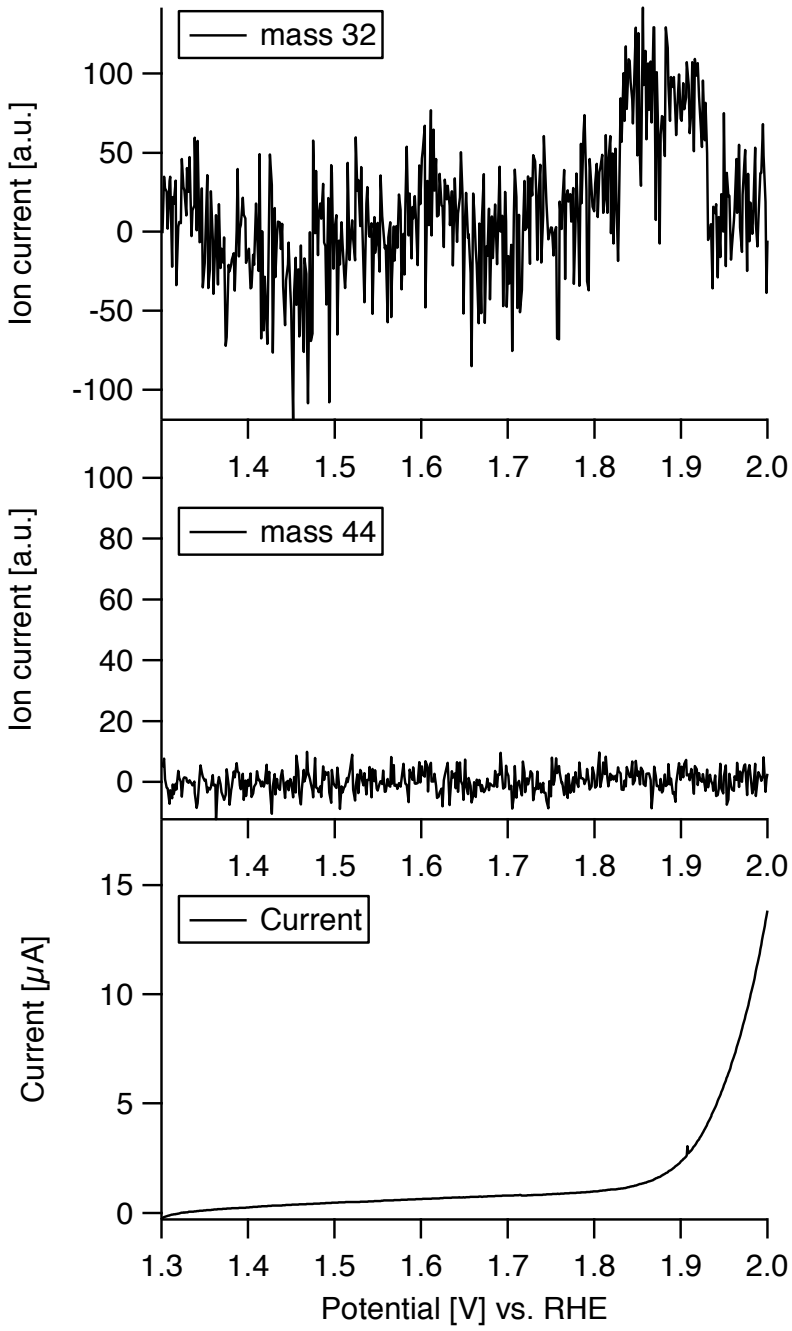

Figure B.6: Results of an OLEMS measurement of a gold working electrode in a 0.1 M Na_2SO_4 solution in the absence of complex **1** (scan range, 1.3-2.0V vs. RHE, scan rate 1 mV/s, starting at 1.3 V vs. RHE). Shown is the forward scan of a CV experiment with the *m/z* trace for O_2 (top), the *m/z* trace for CO_2 (middle) and the corresponding current (bottom).

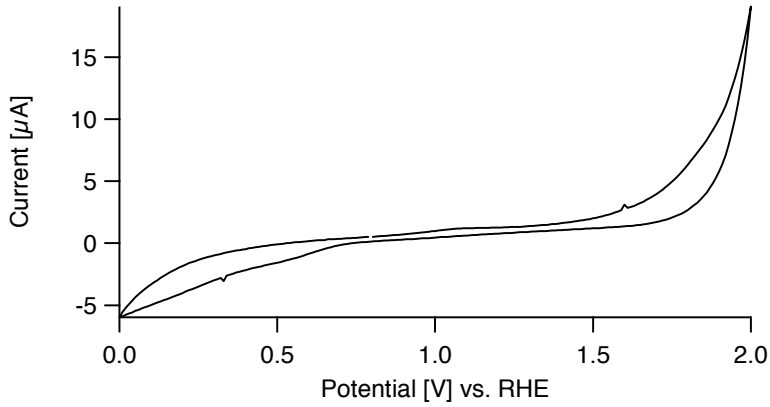

Figure B.7: Voltammogram of 0.5 mM complex **1** in a 0.1 M Na_2SO_4 solution using a BDD working electrode, scanning between 0.0 and 2.0 V vs. RHE at 10 mV/s, starting at 0.7 V vs. RHE

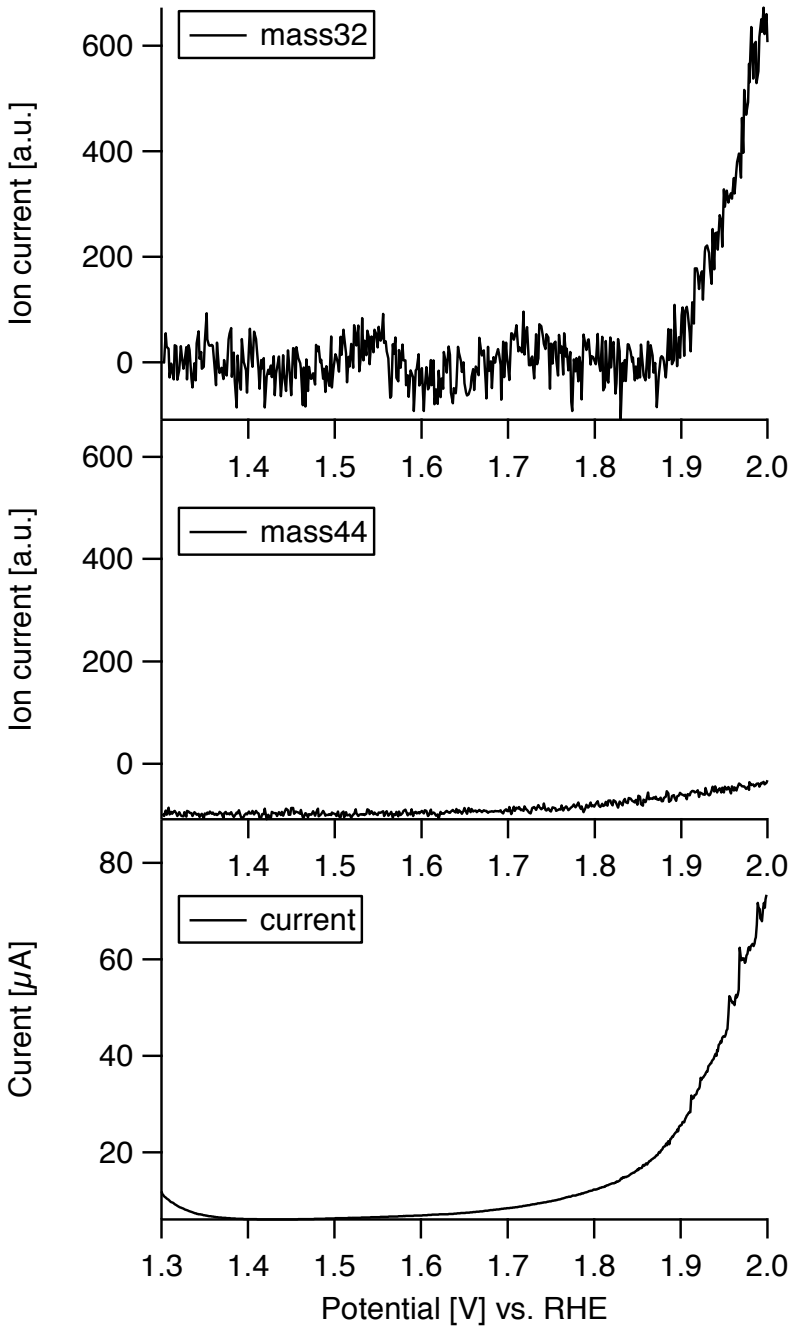

Figure B.8: Results of OLEMS measurement of 1 mM $Fe(OTf)_2$ on a PG working electrode in a 0.1 M Na_2SO_4 solution (scan range, 1.3-2.0V vs. RHE, scan rate 1 mV/s, starting at 1.3 V vs. RHE). Shown is the forward scan of a CV experiment with the *m/z* trace for O_2 (top), *m/z* trace for CO_2 (middle) and the corresponding current (bottom).

Figure B.9: Modified EQCM cell: the top part of the cell was made taller to allow for degassing of the electrolyte solution by bubbling argon. Additionally, a small hole was added to serve as a gas inlet to keep the cell under argon flow during experiments, preventing air from entering.

B.2 Calculation of turnover frequencies

The formula for the calculation of the turnover frequencies in the text of chapter 3 is derived from equation 1 below.[1] With R being the universal gas constant, T being the temperature in Kelvin, F being the Faraday constant and ν being the scan rate in V/s, for a four-electron process (n = 4) such as water oxidation at a room temperature of 293 K this simplifies to equation 2 where the TOF is the same as k_{obs}.

$$\frac{i_{cat}}{i_p} = \frac{n}{0.4463}\sqrt{\frac{RTk_{obs}}{F\nu}} \qquad (1)$$

$$TOF = 0.4848 \cdot \nu \left(\frac{i_{cat}}{i_p}\right)^2 \qquad (2)$$

To calculate the turnover frequency, we used the current of oxidation wave X (cf. Fig. 3.2 and Fig. 3.5, chapter 3) for i_p to calculate the TOF for i_{cat} at different potentials. Background correction was performed to account for the contribution of non-catalytic current to i_{cat}. For the case of complex **1** with a PG working electrode we calculated i_{cat} by subtracting the current of a blank measurement with the same electrode in the absence of complex **1** from the current measured in the presence of complex **1**. For the case of a gold working electrode, however, the contribution of background processes is clearly overlapping with the onset of oxygen evolution, leading to a significant overestimation of i_{cat} at 1.9 and 2.0 V (cf. Fig. 3.2, chapter 3). To eliminate contributions from background processes from i_{cat}, the potential was cycled 5 times between 1.3 and 2.0 V at a scan rate of 10 mV/s with a gold working electrode in the presence of complex **1**. By keeping the potential above 1.3 V, gold oxide reduction is prevented which means that gold oxidation only contributes to the first scan of the experiment. Thus, to determine i_{cat} at 1.9 and 2.0 V, the current of the second scan of the CV experiment between 1.3 and 2.0 V with a gold working electrode in the presence of complex **1** was considered, from which the current of the second scan of an analogous blank experiment with the same gold working electrode in the absence of complex **1** was subtracted.

B.3 Single crystal X-ray crystallography (complex **1**)

All reflection intensities were measured at 110(2) K using a SuperNova diffractometer (equipped with Atlas detector) with Cu *K*α radiation (λ = 1.54178 Å) under the program CrysAlisPro.[2] The same program was used to refine the cell dimensions and for data reduction. The structure was solved with the program SHELXS-2014/7 and was refined on F^2 with SHELXL-2014/7.[3] Analytical numeric absorption correction using a multifaceted crystal model was applied using CrysAlisPro. The temperature of the data collection was controlled using the system Cryojet (manufactured by Oxford Instruments). The H atoms were placed at calculated positions (unless otherwise specified) using the instructions AFIX 43 or AFIX 137 with isotropic displacement parameters having values 1.2 or 1.5 *U*eq of the attached C or N atoms. The H atoms attached to O2 and O3 (coordinated MeOH molecules) were found from difference Fourier maps, and their coordinates were refined freely. The structure is mostly ordered.

Additional Notes:

1. One of the four crystallographically independent triflate counter-ions in the asymmetric unit is found to be disordered over two orientations, and the occupancy factor of the major component of the disorder refines to 0.788(4).

2. The crystal that was mounted on the diffractometer was twinned. The twin relationship corresponds to a twofold axis along the reciprocal vector -0.7007**a*** + 0.7134**b*** -0.0020**c***. The BASF scale factor refines to 0.2164(12). All necessary details about the twin data reduction have been embedded in the .cif file.

Table B.1: Crystallographic data of complex **1**

Identification code	**1**
Crystal data	
Chemical formula	$C_{42}H_{38}Fe_2N_{10}O_3 \cdot 4(CF_3O_3S)$
M_r	1438.80
Space group	Triclinic, *P*-1
Temperature (K)	110
a, *b*, *c* (Å)	11.9405 (5), 12.2853 (4), 20.3054 (6)
α, β, γ (°)	103.183 (3), 102.560 (3), 98.477 (3)
V (Å^3)	2769.26 (18)
Z	2
Radiation type	Cu *K*α
μ (mm^{-1})	6.67
Crystal size (mm)	0.21 × 0.17 × 0.10
Data collection	
Diffractometer	SuperNova, Dual, Cu at zero, Atlas
Absorption correction	Analytical *CrysAlis PRO* 1.171.38.41 Analytical numeric absorption correction using a multifaceted crystal model based on expressions derived by R.C. Clark & J.S. Reid.[2, 4] Empirical absorption correction using spherical harmonics, implemented in SCALE3 ABSPACK scaling algorithm.
T_{min}, T_{max}	0.400, 0.650
No. of measured, independent and observed [$I > 2\sigma(I)$] reflections	35916, 12230, 8520
R_{int}	0.056
$(\sin\theta/\lambda)_{max}$ (Å^{-1})	0.616

Refinement	
$R[F^2 > 2\sigma(F^2)]$, $wR(F^2)$, S	0.054, 0.140, 0.92
No. of reflections	12230
No. of parameters	878
No. of restraints	267
H-atom treatment	H atoms treated by a mixture of independent and constrained refinement
$\Delta\rho_{max}$, $\Delta\rho_{min}$ (e Å^{-3})	0.89, -0.68

Table B.2: Relevant bond distances and angles for complex **1**

Distances (Å)	
Fe1-N1	2.117(4)
Fe1-N2	2.124(4)
Fe1-N4	2.116(4)
Fe1-N5	2.140(4)
Fe1-O1	1.782(3)
Fe1-O2	2.147(3)
Fe2-N6	2.133(4)
Fe2-N7	2.114(4)
Fe2-N10	2.125(4)
Fe2-N11	2.112(4)
Fe2-O1	1.778(3)
Fe2-O3	2.147(3)
C1-C25	4.339(7)
C4-C27	3.829(8)
C6-C30	3.515(6)
C10-C31	3.365(6)
C11-C35	3.445(6)
C14-C37	3.376(6)
C16-C40	3.552(6)
Bond angles (°)	
N1-Fe1-N2	78.15(15)
N2-Fe1-N4	87.12(15)
N4-Fe1-N5	78.74(15)
N1-Fe1-N5	114.25(15)
N6-Fe2-N7	78.46(15)
N7-Fe2-N10	86.96(15)
N10-Fe2-N11	78.42(14)
N6-Fe2-N11	114.57(15)
Fe1-O1-Fe2	155.78(18)
Torsion angles (°)	
C19-C12-C9-C2	-16.4(1)
C39-C32-C29-C22	-3.0(1)
N3-Fe1-Fe2-N9	-44.0(1)

B.4 References

[1] J. M. Saveant; E. Vianello, *Electrochim. Acta* **1965**, *10*, 905-920.
[2] O. D. Rigaku *CrysAlisPro*, version 1.171.38.41; Rigaku Oxford Diffraction: Oxford, UK, 2015.
[3] G. M. Sheldrick, *Acta Crystallogr., Sect. C: Struct. Chem.* **2015**, *71*, 3-8.
[4] R. C. Clark; J. S. Reid, *Acta Crystallogr., Sect. A: Found. Adv.* **1995**, *51*, 887-897.

Appendix C

Supplementary information for Chapter 4

Figure C.1: Formation of solid precipitate inside the electrochemical cell during electrochemical measurements of complex **2** in 0.1 M $HClO_4$

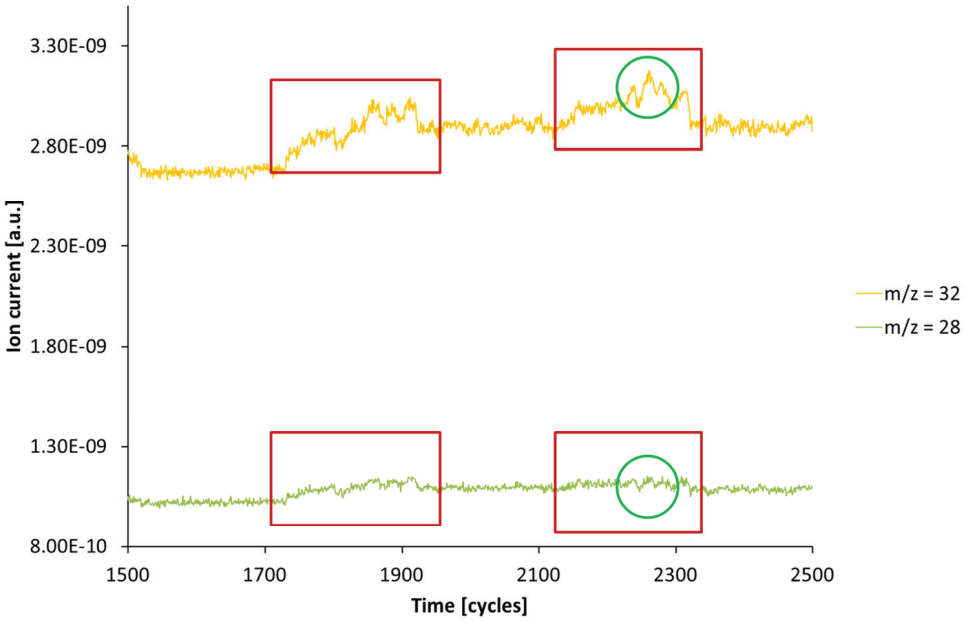

Figure C.2: Examples of the artefacts present in OLEMS measurements. The yellow trace represents the response for *m/z* = 32, the green trace represents the response for *m/z* = 28. The red boxes indicate noise which can be seen in both mass traces and therefore does not correspond to actual oxygen evolution while the green circles show real oxygen signals caused by complex **2** which are therefore absent in the trace of *m/z* = 28.

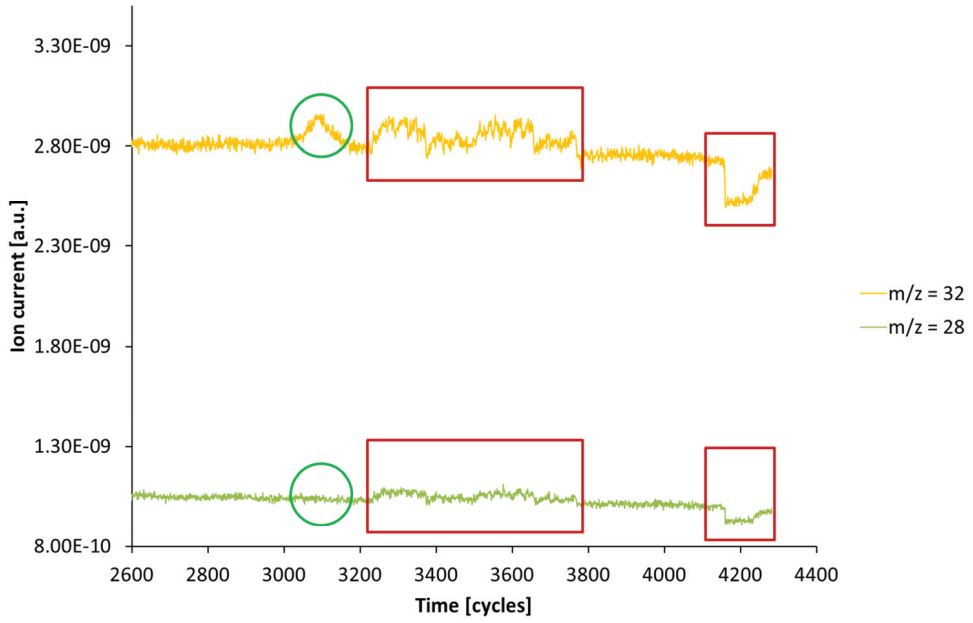

Figure C.3: Examples of the artefacts present in OLEMS measurements. The yellow trace represents the response for *m/z* = 32, the green trace represents the response for *m/z* = 28. The red boxes indicate noise which can be seen in both mass traces and therefore does not correspond to actual oxygen evolution while the green circles show real oxygen signals caused by complex **2** which are therefore absent in the trace of *m/z* = 28.

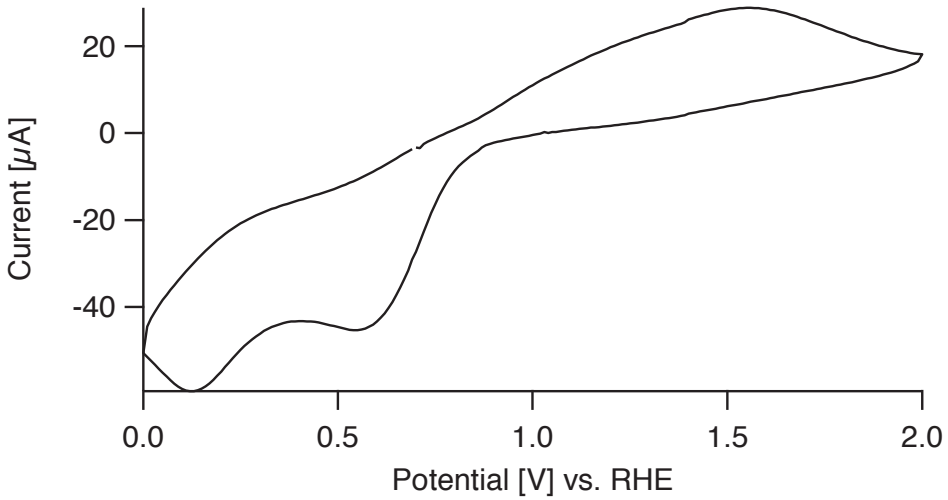

Figure C.4: Voltammogram of 1.1 mM complex **3** in a 0.1 M Na_2SO_4 electrolyte solution, recorded between 0.0 and 2.0 V vs. RHE at 100 mV/s with an ITO working electrode, starting at 0.7 V vs. RHE.